Check for updates

Visible light communications: multi-band super-Nyquist CAP modulation

P. A. HAIGH,[1,4] **P. CHVOJKA,**[2,4] **Z. GHASSEMLOOY,**[3] **S. ZVANOVEC,**[2] **AND I. DARWAZEH**[1,*]

[1]*Communications and Information Systems Group, University College London, WC1E 6BT London, UK*
[2]*Department of Electromagnetic Field, Faculty of Electrical Engineering, Czech Technical University in Prague, Technicka 2, 16627, Prague, Czech Republic*
[3]*Optical Communications Research Group, Faculty of Engineering and Environment, Northumbria University, NE1 8ST, UK*
[4]*These authors contributed equally*
[*]*i.darwazeh@ucl.ac.uk*

Abstract: In this paper, we experimentally demonstrate the performance of a non-orthogonal multi-band super-Nyquist carrier-less amplitude and phase (m-SCAP) modulation for visible light communications (VLC). We break the orthogonality between sub-bands in the frequency domain by compressing the spectrum, purposely overlapping them, and introducing inter-band interference (IBI). We demonstrate that our proposed system can tolerate IBI, and hence spectral efficiency can be increased without introducing additional complexity to the receiver. We show that m-SCAP can tolerate up to 30% and 20% compression for 4- and 16-level quadrature amplitude modulation, respectively, thus leading to an improvement in spectral efficiencies up to 40% and 25%, respectively, at the cost of bit error rate performance, which however remains below the 7% forward error correction limit. Moreover, the experimental results are supported by numerical simulations.

1. Introduction

The need for communication systems using modulation schemes that offer high spectral efficiency is evident especially due to the ever-increasing end-user demands for high-speed data services [1]. Within this context, there has recently been growing research interest in carrier-less amplitude and phase (CAP) modulation as a possible alternative candidate to orthogonal frequency division multiplexing (OFDM) for future high-speed visible light communication (VLC) systems [2–4], particularly with the extension to a multi-band CAP (m-CAP) scheme [5,6]. In VLC systems, the maximum achievable transmission data rate is mostly limited by the inherent modulation bandwidth of light-emitting diodes (LEDs) [7,8], therefore effective utilisation of the LED's bandwidth B_{LED} is a major priority to increase data rate R_b. In [6] it was shown that spectral efficiency η_{se} gains could be achieved by means of frequency division multiplexing within the CAP signal bandwidth B_{CAP}, dividing it into increasingly small, evenly m distributed sub-bands. Spectral efficiency gains can be obtained since reduction of the sub-band bandwidth introduces increased resilience against the low-pass frequency response of the LED. As such, the total attenuation experienced by each sub-band is reduced, and therefore each sub-band can be approximated as a flat-band. Furthermore, adaptive bit-loading can be introduced to the system where each sub-band can transmit a higher number of bits-per-symbol in comparison to the conventional 1-CAP system.

The m-CAP scheme has been widely adopted in VLC systems [9–14] and has subsequently been demonstrated in many new methods. In a generic formulation of m-CAP such as in [6], each sub-band has an equivalent bandwidth. Considering B_{LED} and B_{CAP} are independent, and very often in VLC $B_{CAP} > B_{LED}$ [15], a number of m-CAP schemes have been proposed that vary the

individual sub-band bandwidths according to these two quantities [9, 11]. In [9], it was proposed to maintain the condition $B_{CAP} > B_{LED}$ and divide m sub-bands into two categories; (*i*) those within a DC-B_{LED} frequency range; and (*ii*) those beyond B_{LED}. By setting the bandwidth of the first sub-band equal to B_{LED} and dividing the remaining $(m-1)$ sub-bands across the excess frequency range, a data rate gain of 36% could be obtained. This was also confirmed in [11] for a different system, where adopting a similar approach as in [9] resulted in 80% reduction of the number of real-valued multiplications at the cost of a marginally higher signal-to-noise ratio (SNR) penalty. The m-CAP format also enables straightforward multiple-access capabilities, where sub-bands can be assigned to users depending on their requirements [12].

It is still possible to further increase the spectral efficiency of m-CAP systems. One of the best methods to achieve this is to reduce the spacing between sub-bands, by intentionally violating the frequency-domain orthogonality between sub-bands, thus introducing pre-determined inter-band interference (IBI). This draws inspiration from the methodology proposed in other non-orthogonal frequency-domain modulations, particularly spectrally efficient FDM (SEFDM) [16, 17]. In SEFDM, the subcarrier spacing is compressed beyond the orthogonality limit, hence resulting in high inter-carrier interference (ICI), and increased spectral efficiency at the cost of increased computational complexity at the receiver. The same idea has been translated into the time-domain in the form of faster-than-Nyquist signalling [18], where an improvement in spectral efficiency is achieved by intentional aliasing of pulse shaping filters at the cost of introducing inter-symbol interference (ISI). In these systems, knowledge of the interference characteristics allows amelioration of interference effects at the receiver and in SEFDM this has resulted in the demonstration of systems that can increase throughput by up to 60% with a tolerable loss of performance [19–22]. Such an approach has already been applied to m-CAP as reported in the literature [10, 23] and was termed non-orthogonal m-CAP (NM-CAP) in [23] and super-Nyquist CAP in [10]. In [23] it was reported that the performance gains can be achieved by overlapping subcarriers for 4-level quadrature amplitude modulation (4-QAM) and 10 sub-bands, thus resulting in a 44% increase in spectral efficiency. For all intents and purposes, super-Nyquist is intended to mean the baud rate is far in excess of the bandwidth occupied in this paper, as in [24]. In [10] it was shown that the IBI can be modelled as a multiple-input multiple-output system and hence, a least mean square Volterra-based equaliser is capable of recovering the transmitted symbols from two sub-bands. For simplicity of nomenclature, to consolidate terms between the two reports, we herein adopt the term multi-band super-Nyquist CAP (m-SCAP). In this paper, we extend the studies on super-Nyquist CAP for 4- and 16-QAM VLC links by investigating the bit-error rate (BER) performance for $m = 2$ to 10 and a varying the sub-band compression factor α up to 50%. There are several key differences from our previous work reported in [23], in particular, the results shown are based on the total achievable BER performance of the system, while [23] focuses on the individual sub-band performance. We show that by reducing the spacing between individual sub-bands spectral efficiency gains of up to 40% can be achieved. The results are demonstrated experimentally and validated by numerical simulations.

2. Multi-band super-Nyquist CAP

In this section, we outline the theoretical framework adopted to design and implement the proposed m-SCAP system as shown in Fig. 1. A set of m pseudorandom binary sequences, each of length $2^{15} - 1$, denoted as $\mathbf{D_1}$ to $\mathbf{D_m}$ are generated for the respective 1st to mth sub-bands, prior to being mapped into the M-QAM constellation, where $M = 4$ and 16. Next, the modulated signals are split into their real and imaginary components before being up-sampled based on the number of samples-per-symbol $N_{ss} = \xi \lceil 2m(1+\beta) \rceil$, where ξ is an over-sampling factor set to 2 in this work with no loss of generality and β is the excess bandwidth factor of the square-root raised cosine (SRRC) that forms the basis of the pulse shaping filters. The final pulse shaping filters are given by the product of the SRRC with a cosine (in-phase $p(t)$) and a sine (quadrature
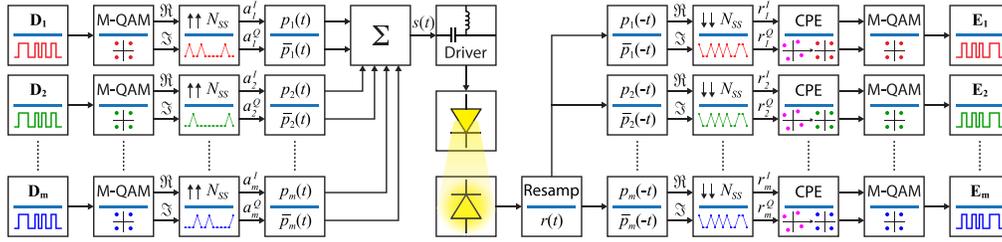
Fig. 1. The schematic block diagram of the m-SCAP system under test.

$\bar{p}(t)$), given by [5,6]:

$$p_n(t) = \left[\frac{\sin\left(\pi \frac{t}{T_s}[1-\beta]\right) + 4\beta \frac{t}{T_s} \cos\left(\pi \frac{t}{T_s}[1+\beta]\right)}{\pi \frac{t}{T_s}\left[1 - \left(4\beta \frac{t}{T_s}\right)^2\right]} \right] \cos\left(2\pi f_{c,n} \frac{t}{T_s}\right) \tag{1}$$

$$\bar{p}_n(t) = \left[\frac{\sin\left(\pi \frac{t}{T_s}[1-\beta]\right) + 4\beta \frac{t}{T_s} \cos\left(\pi \frac{t}{T_s}[1+\beta]\right)}{\pi \frac{t}{T_s}\left[1 - \left(4\beta \frac{t}{T_s}\right)^2\right]} \right] \sin\left(2\pi f_{c,n} \frac{t}{T_s}\right) \tag{2}$$

It is clear from Eqs. (1) and (2) that the dependence on the nth sub-band is present in the multiplication with the cosine and sine terms, which are responsible for the up-conversion. The carrier frequency is given by $f_{c,n}$ where $n = 0, \ldots, m - 1$, can be expressed as:

$$f_{c,n} = \frac{B_{CAP}}{2m} - \frac{n\left[\frac{B_{CAP}}{m} + B_{CAP}(\alpha - 1)\right]}{m - 1} \tag{3}$$

recalling that B_{CAP} is the total bandwidth of the entire signal and m is the total number of sub-bands.

In Eq. (4) we introduce the term α that corresponds to the compression of the sub-bands, which intentionally causes overlapping between them in a fashion analogous to that of SEFDM [22]. The data is then applied to the pulse shaping filters the outputs of which are summed together as given by [5,6]:

$$s(t) = \sum_{n=1}^{m} \left[a_n^I(t) \otimes p_n(t) - a_n^Q \otimes \bar{p}_n(t) \right] \tag{4}$$

where $\otimes$ denotes time-domain convolution, a_n^I and a_n^Q are the in-phase and quadrature up-sampled M-QAM symbols transmitted by the nth sub-band.

The concept of the proposed scheme is illustrated in Fig. 2. Examples of conventional orthogonal m-CAP are shown in Figs. 2(a) and (b) for $m = 2$ and for $\beta = 0.1$ and 0.5, which offer negligible IBI (i.e. orthogonality). Starting with a 2-SCAP system, Figs. 2(c) and (d) show the ideal spectra of the proposed compressed system (blue) and the contributions of each of sub-band for $\alpha = 0.2$, i.e. 20% compression. Note that sub-band overlapping results in a 6 dB (electrical) power penalty observed at the interface. In [6], it was reported that increasing the order of m resulted in improved performance due to the alleviation of the high-frequency attention introduced by the LED [6], and hence in this work, we have used up 10 sub-bands. Note that, it is expected that a 2-SCAP VLC system would offer improved performance in comparison to higher order systems. This is because each sub-band only has a single interferer, while in higher order

systems every sub-band (except the first and the last) is affected by interferers on either side. On the other hand, for high values of m and β (see Figs. 2(e) and (f)) we observe that; (*i*) the relative sub-band overlap decreases with increasing m, i.e. for 2- and 10-CAP the relative overlaps are 20% and 12.5%, respectively; and (*ii*) the attenuation between sub-bands actually decreases to be approximately equal to the power of the main sub-band, due to the excess bandwidth and shallower gradient of the frequency roll-off. Hence, we note that there is a trade-off between the level of IBI and the baud rate relating to the excess bandwidth factor as $R_s = B_{CAP}/(1 + \beta)$.
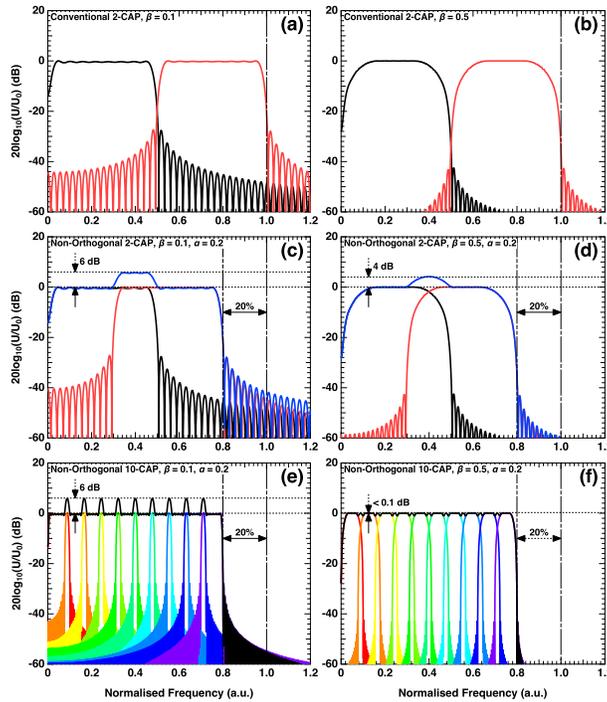
Fig. 2. Conventional 2-CAP for: (a) $\beta = 0.1$, and (b) $\beta = 0.5$; the proposed m-SCAP scheme for: (c) $m = 2$, $\beta = 0.1$, $\alpha = 0.2$, (d) $m = 2$, $\beta = 0.5$, $\alpha = 0.2$, (e) $m = 10$, $\beta = 0.1$, $\alpha = 0.2$, and (f) $m = 10$, $\beta = 0.5$, $\alpha = 0.2$.

As outlined, the main motivation behind compressing the sub-bands is to increase η_{se}, which is given by [23]:

$$\eta_{se} = \frac{k}{(1 + \beta)(1 - \alpha)} \qquad (5)$$

where k is the number of bits/symbol. Note that by compressing the sub-bands beyond their orthogonality limit, it will be possible to increase η_{se} without increasing the computational complexity of the receiver at the cost of increased BER.

The generated signal $s(t)$ samples were loaded into a vector signal generator (Rhode & Schwarz SMW200A) prior to intensity modulation of an LED (Osram Golden Dragon). Note, the white phosphor LED has a measured frequency response of $\sim$ 1 MHz with a band-pass filter like transfer function because of the bias-tee used as part of the LED driver. The focus of this work is not to increase the transmission speed but to investigate the performance of overlapping individual sub-bands in m-CAP, and hence, it was not deemed necessary to extend the bandwidth of the LED beyond 1 MHz, while we set the signal bandwidth to 3 MHz for comparison with our previous work [23]. The LED bias current was set to 500 mA, which is approximately the midway point of the linear operating region of the L-I-V transfer function, thus ensuring maximum symmetrical

swing of the modulating signal. The distance between the transmitter and receiver was set to 2 m, i.e. a realistic link span in the home/office environment.

At the receiver, a low-noise avalanche photodiode with in-built trans-impedance amplifier (Thorlabs APD430A2/M) was used to convert the optical signal back to the electronic domain. Two 25.4 mm biconvex lenses (not shown in Fig. 1 for simplicity) were used to collimate and focus the light beam, one at the transmitter placed at a distance of 25 mm and one at the receiver at a distance of 35 mm. The received optical power at the receiver is 1.5 mW.

The regenerated electrical signal was then captured using a real-time oscilloscope (LeCroy WaveRunner Z640i) at a sampling rate of 50 MSa/s for further processing in MATLAB. The demodulation process is the same as that of conventional m-CAP [6]. That is, the received data is resampled to that of the original sampling frequency before transmission, which is given by $f_s = R_s N_{ss} m^{-1}$. Subsequently, the signal is passed through time-reversed matched filters for each sub-band prior to down-sampling at N_{ss} and common phase error (CPE) correction in the standard manner. Finally, the symbols are de-mapped from the relevant M-QAM constellation and buffered to create a vector estimate of the nth transmitted bit vector $\mathbf{E_n}$, which is then used for BER measurements, i.e. directly comparing $\mathbf{E_n}$ and $\mathbf{D_n}$ at the bit level. Note, the entire transmission and reception process was automated using MATLAB. Furthermore, to understand the fundamental limits that the IBI causes on system performance and to maintain the simplest possible receiver, no equalisation scheme is used.

3. Results and discussion

In this section, we present experimental results for the total BER of the system as a function of m and α for each value of β and k. The total BER is determined by the summation of the total number of errors on each sub-band divided by the total number of bits transmitted across all sub-bands. Note, the BER floor is set to 10^{-4} based on $\sim 30,000$ bits for each sub-band, corresponding to a confidence level $> 95\%$ [25].

In order to validate the experimentally measured BER results, we carried out a numerical simulation in MATLAB, which used the measured system responses (i.e. L-I-V curve and the bandwidth as given in [23], as well as the signal-to-noise ratio (SNR) of ~ 19.5 dB measured experimentally). Figure 3 depicts the total measured (solid lines) and simulated (dashed lines) BER performance as a function of α for a range of m, k and β showing a good agreement. Note, the m-SCAP BER performance improves with increasing m particularly for a compression $\alpha < 30\%$. This improvement in the BER performance is attributed to the fact that the signal with a bandwidth of 3 MHz is transmitted within the stop-band of the LED (i.e. B_{LED} of 1.1 MHz). Therefore the SNR improvement gained by increasing m (refer to [6]) actually becomes dominant when considering the increase in IBI from more than one source for $m > 2$. Note, higher m-SCAP (i.e., ≥ 8) can support α of 30%, which corresponds to a saving in the bandwidth of 900 kHz. Note that we measured an increase in η_{se} from 1.33 b/s/Hz in the uncompressed case using Eq. (5) to 1.9 b/s/Hz, for $m = 8$, $k = 2$ bits/symbol, $\alpha = 30\%$ and $\beta = 0.5$, which represents a significant improvement of over 40%. This implies that the same transmission speed can be supported using a lower bandwidth, which is reduced by 30%. Therefore, the overall data rate can be increased by utilising the unused bandwidth for transmission of additional information. Also note, for $\alpha \geq 0.4$, the BER values are above the FEC limit. This is because the IBI interference is the dominant noise source and cannot be reduced using the hard threshold detection scheme, although using advanced equalisers it may be possible.

As shown in Fig. 3(a), which offers the highest level of compression, it is clear that for $k = 2$ bits/symbol and $\beta = 0.5$ every system, i.e. any m, can support compression of at least 20% (i.e. $\alpha = 0.2$) whilst maintaining a total BER below the 7% forward error correction (FEC) limit of 3.8×10^{-3}. The measured BER results (solid line) show that the worst performance is offered by 2-CAP, given that each of the sub-bands only interferes with each other. This can

be observed for all systems tested. The BER results for $k = 2$ and $\beta = 0.3$, see Fig. 3(b), show a reduction in a possible bandwidth compression in comparison to Fig. 3(a), since the highest compression is now $\alpha = 0.2$ for every number of sub-bands, except $m = 2$, which can only support $\alpha = 0.1$. However, since the excess bandwidth factor is reduced, η_{se} is slightly increased to 1.92 b/s/Hz, showing a marginal improvement over the previous case. Interestingly, for a given BER a lower number of sub-bands are required to achieve $\eta_{se} = 1.92$ b/s/Hz, that is $m = 4$ for $\beta = 0.3$, $\alpha = 0.2$ and $m = 8$ and 10 for $\beta = 0.5$ and $\alpha = 0.3$, which advantageously reduces the computational complexity by at least half [26].

As depicted in Fig. 3(c) for $\beta = 0.1$ and $k = 2$ the largest compression supported was $\alpha = 0.1$ for all m except $m = 2$, which can only support the uncompressed case at a BER value below the FEC limit. However, even though this is the smallest compression factor reported here, it corresponds to $\eta_{se} = 2.02$ b/s/Hz, i.e. the highest η_{se} for $k = 2$. The reason for α decreasing with β is the availability of reduced excess bandwidth, i.e. a steeper roll-off of the magnitude response of the filter and hence, a smaller inter-band guard slot and consequently the IBI dominates even for lower values of α.
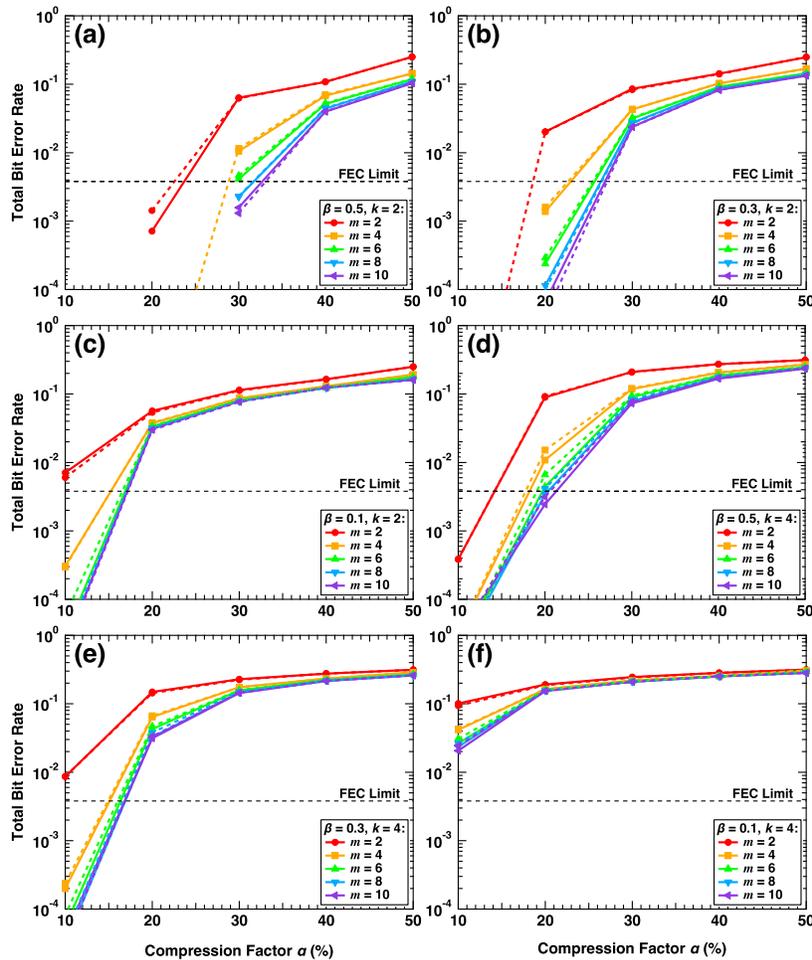
Fig. 3. Measured (solid lines) and simulated (dashed lines) total BER of m-SCAP as a function of m and β for Figs. 3(a)–(c) $k = 2$ and Figs. 3(d)–(f) $k = 4$.

Figure 3(d) illustrates the BER performance for $k = 4$ and $\beta = 0.5$, where $\alpha \leq 20\%$ can be

supported to achieve a BER below the FEC limit only for $m \geq 8$. This indicates a clear reduction from the $k = 2$ case, where $\alpha = 0.3$ could be supported. This is clearly due to the additional SNR requirements in order to increase the modulation alphabet size from $M = 4$ to $M = 16$. Note that $\eta_{se} = 3.33$ b/s/Hz and 2.67 b/s/Hz can be supported for the system with and without compression, respectively, which corresponds to an increase of around 0.6 b/s/Hz or 25% with no additional complexity at the receiver. Figure 3(e) depicts the BER plots for $\beta = 0.3$ and $k = 4$. For a BER below the FEC limit, a compression factor of $\alpha = 10\%$ is supported for all m except for $m = 2$. In this case, following compression $\eta_{se} = 3.42$ b/s/Hz was achieved, which is the highest value reported for $k = 4$. In comparison to η_{se} of 2.67 b/s/Hz for the uncompressed case, this is an improvement of 0.75 b/s/Hz (i.e., $\sim 22\%$). As was the case for $k = 2$, the m-SCAP link with $k = 4$ can be supported for $m = 4$ instead of $m > 8$ to achieve approximately the same η_{se}, while maintaining the 50% reduction in computational complexity as only half the number of FIR filters are required. Finally, for $\beta = 0.1$, no link can be supported with a BER below the FEC limit – see Fig. 3(f).

Figure 4 illustrates the spectral profiles for $k = 2$ and 4, which offer the highest spectral efficiencies, i.e. $k = 2$, $m = 4$, $\beta = 0.1$, and $\alpha = 0.1$ as well as $k = 4$, $m = 4$, $\beta = 0.3$, and $\alpha = 0.1$, respectively, together with constellations inset for each sub-band. Note that the spectral overlap is shown in the black colour.
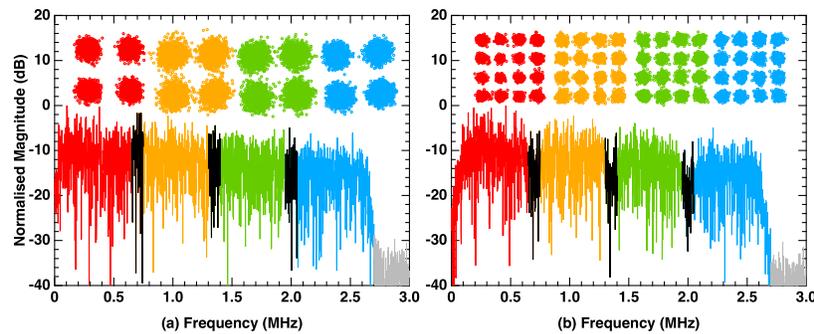
Fig. 4. Electrical spectra and constellations for the highest spectral efficiency systems for (a) $k = 2$, $m = 4$, $\beta = 0.1$, $\alpha = 0.1$ and (b) $k = 4$, $m = 4$, $\beta = 0.3$, $\alpha = 0.1$.

4. Conclusion

This paper presented experimental results for the proposed m-SCAP system, which is verified by means of numerical simulations. We showed that by varying the filter parameters and number of sub-bands, the spectrum can be compressed by up to 30%, thus resulting in an increased spectral efficiency by $< 40\%$. We also showed that an improvement in spectral efficiency can be achieved in the absence of any optimisation on the allocation of bits/power to each sub-band or by introducing additional complexity at the receiver. Finally, we demonstrated that both 4-QAM and 16-QAM constellations can be supported with compressed spectrums.

References

1. Cisco, "Cisco visual networking index: Global mobile data traffic forecast update, 2013-2018," (2014).
2. Y. G. Wang, X. X. Huang, L. Tao, J. Y. Shi, and N. Chi, "4.5-Gb/s RGB-LED based WDM visible light communication system employing CAP modulation and RLS based adaptive equalization," Opt. Express **23**, 13626–13633 (2015).
3. Y. G. Wang, L. Tao, X. X. Huang, J. Y. Shi, and N. Chi, "8-Gb/s RGBY LED-based WDM VLC system employing high-order CAP modulation and hybrid post equalizer," IEEE Photonics J. **7**, 1–7 (2015).
4. F. M. Wu, C. T. Lin, C. C. Wei, C. W. Chen, Z. Y. Chen, H. T. Huang, and S. Chi, "Performance comparison of OFDM signal and CAP signal over high capacity RGB-LED-based WDM visible light communication," IEEE Photonics J. **5**, 7901507–7901507 (2013).
5. M. I. Olmedo, T. J. Zuo, J. B. Jensen, Q. W. Zhong, X. G. Xu, S. Popov, and I. T. Monroy, "Multiband carrierless amplitude phase modulation for high capacity optical data links," J. Light. Technol. **32**, 798–804 (2014).
6. P. A. Haigh, A. Burton, K. Werfli, H. L. Minh, E. Bentley, P. Chvojka, W. O. Popoola, I. Papakonstantinou, and S. Zvanovec, "A multi-CAP visible-light communications system with 4.85-b/s/Hz spectral efficiency," IEEE J. on Sel. Areas Commun. **33**, 1771–1779 (2015).
7. P. A. Haigh, Z. Ghassemlooy, S. Rajbhandari, I. Papakonstantinou, and W. Popoola, "Visible light communications: 170 Mb/s using an artificial neural network equalizer in a low bandwidth white light configuration," J. Light. Technol. **32**, 1807–1813 (2014).
8. Z. Ghassemlooy, L. Alves, M. Khalighi, and S. Zvanovec, *Visible Light Communications: Theory and Applications* (Taylor & Francis Incorporated, 2017).
9. P. Chvojka, S. Zvanovec, K. Werfli, P. A. Haigh, and Z. Ghassemlooy, "Variable *m*-CAP for bandlimited visible light communications," in *IEEE International Conference on Communications Workshops, ICC Workshops 2017,* (IEEE, 2017), pp. 1–5.
10. S. Liang, L. Qiao, X. Lu, and N. Chi, "Enhanced performance of a multiband super-Nyquist CAP-16 VLC system employing a joint MIMO equalizer," Opt Express **26**, 15718–15725 (2018).
11. K. Werfli, P. A. Haigh, Z. Ghassemlooy, N. B. Hassan, and S. Zvanovec, "A new concept of multi-band carrier-less amplitude and phase modulation for bandlimited visible light communications," in *2016 10th International Symposium on Communication Systems, Networks and Digital Signal Processing (CSNDSP),* (IEEE, 2016), pp. 1–5.
12. M. M. Merah, H. Guan, and L. Chassagne, "Performance optimization in multi-user multiband carrierless amplitude and phase modulation for visible light communication," in *2018 Global LIFI Congress (GLC),* (IEEE, 2018), pp. 1–4.
13. Y. Wang, L. Tao, Y. Wang, and N. Chi, "High speed wdm VLC system based on multi-band CAP-64 with weighted pre-equalization and modified CMMA based post-equalization," IEEE Commun. Lett. **18**, 1719–1722 (2014).
14. K. O. Akande and W. O. Popoola, "Subband index carrierless amplitude and phase modulation for optical communications," J. Light. Technol. **36**, 4190–4197 (2018).
15. N. Chi, M. J. Zhang, J. Y. Shi, and Y. H. Zhao, "Spectrally efficient multi-band visible light communication system based on nyquist PAM-8 modulation," Photonics Res. **5**, 588–597 (2017).
16. I. Kanaras, A. Chorti, M. R. Rodrigues, and I. Darwazeh, "Spectrally efficient FDM signals: Bandwidth gain at the expense of receiver complexity," in *IEEE International Conference on Communications,* (IEEE, 2009).
17. M. Rodrigues and I. Darwazeh, "A spectrally efficient frequency division multiplexing based communications system," in *Proceedings of the 8th International OFDM-Workshop,* (IEEE, 2003), pp. 70–74.
18. J. B. Anderson, F. Rusek, and V. Owall, "Faster-than-nyquist signaling," Proc. IEEE **101**, 1817–1830 (2013).
19. I. Darwazeh, T. Y. Xu, T. Gui, Y. Bao, and Z. H. Li, "Optical SEFDM system; bandwidth saving using non-orthogonal sub-carriers," IEEE Photonics Technol. Lett. **26**, 352–355 (2014).
20. D. Nopchinda, T. Y. Xu, R. Maher, B. C. Thomsen, and I. Darwazeh, "Dual polarization coherent optical spectrally efficient frequency division multiplexing," IEEE Photonics Technol. Lett. **28**, 83–86 (2016).
21. T. Y. Xu, S. Mikroulis, J. E. Mitchell, and I. Darwazeh, "Bandwidth compressed waveform for 60-GHz millimeter-wave radio over fiber experiment," J. Light. Technol. **34**, 3458–3465 (2016).
22. I. Darwazeh, H. Ghannam, and T. Xu, "The first 15 years of SEFDM: A brief survey," in *11th International Symposium on Communication Systems, Networks and Digital Signal Processing (CSNDSP),* (IEEE, 2018), pp. 1–5.
23. P. A. Haigh, P. Chvojka, Z. Ghassemlooy, S. Zvanovec, and I. Darwazeh, "Non-orthogonal multi-band CAP for highly spectrally efficient VLC systems," in *11th International Symposium on Communication Systems, Networks & Digital Signal Processing (CSNDSP),* (IEEE, 2018), pp. 1–6.
24. J. J. Yu, J. W. Zhang, Z. Dong, Z. S. Jia, H. C. Chien, Y. Cai, X. Xiao, and X. Y. Li, "Transmission of 8×480-gb/s super-nyquist-filtering 9-qam-like signal at 100 ghz-grid over 5000-km smf-28 and twenty-five 100 ghz-grid roadms," Opt. Express **21**, 15686–15691 (2013).
25. M. C. Jeruchim, P. Balaban, and K. S. Shanmugan, *Simulation of communication systems: modeling, methodology and techniques* (Springer Science & Business Media, 2006).
26. J. Wei, C. Sanchez, P. A. Haigh, and E. Giacoumidis, "Complexity comparison of multi-band CAP and DMT for practical high speed data center interconnects," in *Asia Communications and Photonics Conference,* (Optical Society of America, 2017), p. M2G. 4.